MNRAS 000, 1–6 (2017) Preprint April 10, 2017 Compiled using MNRAS LATEX style file v3.0

New ALMA constraints on the star-forming ISM at low metallicity: A 50 pc view of the blue compact dwarf galaxy SBS 0335−052

D. Cormier[1]★, G. J. Bendo[2], S. Hony[1], V. Lebouteiller[3], S. C. Madden[3], F. Galliano[3], S. C. O. Glover[1], R. S. Klessen[1], N. P. Abel[4], F. Bigiel[1], and P. C. Clark[5]

[1] *Institut für theoretische Astrophysik, Zentrum für Astronomie der Universität Heidelberg, Albert-Ueberle Str. 2, 69120 Heidelberg, Germany*
[2] *Jodrell Bank Centre for Astrophysics, School of Physics and Astronomy, The University of Manchester, Oxford Road, Manchester M13 9PL, UK*
[3] *Laboratoire AIM, CEA/DSM - CNRS - Université Paris Diderot, Irfu/Service d'Astrophysique, CEA Saclay, 91191 Gif-sur-Yvette, France*
[4] *University of Cincinnati, Clermont College, Batavia, OH, 45103, USA*
[5] *School of Physics and Astronomy, Queen's Buildings, The Parade, Cardiff University, Cardiff, CF24 3AA, UK*

arXiv:1702.08467v2 [astro-ph.GA] 7 Apr 2017

Accepted 2017 February 24. Received 2017 February 23; in original form 2016 December 2

ABSTRACT

Properties of the cold interstellar medium of low-metallicity galaxies are not well-known due to the faintness and extremely small scale on which emission is expected. We present deep ALMA band 6 (230 GHz) observations of the nearby, low-metallicity ($12 + \log(O/H) = 7.25$) blue compact dwarf galaxy SBS 0335−052 at an unprecedented resolution of 0.2 arcsec (52 pc). The ^{12}CO J=2→1 line is not detected and we report a 3-σ upper limit of $L_{CO(2-1)} = 3.6 \times 10^4$ K km s^{-1} pc^2. Assuming that molecular gas is converted into stars with a given depletion time, ranging from 0.02 to 2 Gyr, we find lower limits on the CO-to-H2 conversion factor α_{CO} in the range $10^2 - 10^4$ M$_\odot$ pc^{-2} (K km s^{-1})$^{-1}$. The continuum emission is detected and resolved over the two main super star clusters. Re-analysis of the IR-radio spectral energy distribution suggests that the mm-fluxes are not only free-free emission but are most likely also associated with a cold dust component coincident with the position of the brightest cluster. With standard dust properties, we estimate its mass to be as large as 10^5 M$_\odot$. Both line and continuum results suggest the presence of a large cold gas reservoir unseen in CO even with ALMA.

Key words: galaxies: dwarf – galaxies: star formation – galaxies: individual: SBS 0335−052 – submillimeter: ISM

1 INTRODUCTION

Star-formation conditions in low-metallicity environments are not well known due to the lack of observational constraints on the cold dust and gas. Recent efforts with ground-based telescopes have tried to detect the cold gas reservoirs through carbon monoxide (CO) in nearby low-metallicity galaxies (e.g., Schruba et al. 2012; Elmegreen et al. 2013; Cormier et al. 2014; Hunt et al. 2015; Rubio et al. 2016). CO emission is found to be weak in those galaxies while active, bursty star formation is often evident. This would imply significantly different star-formation efficiencies unless CO no longer traces the bulk of the star-forming gas. Star formation taking place in the atomic gas (e.g., Glover & Clark 2012; Krumholz 2012) as well as changes in the standard CO-to-H_2 conversion factor between high- and low-metallicity galaxies have been suggested (see the review by Bolatto et al. 2013) though the amplitude of those changes is unknown. A complementary probe of the ISM in galaxies comes from the continuum emission. Recent, sensitive observations in the far-IR/millimeter (mm) with *Herschel* (Pilbratt et al. 2010) have allowed us to constrain the spectral energy distributions (SEDs) of many nearby low-metallicity dwarf galaxies and to derive more robust dust masses (e.g., Rémy-Ruyer et al. 2015). However, most galaxies with metallicities ≤1/5 $Z_\odot$ remain undetected in the submm/mm regime, implying that characterizations of a possible cold (T_{dust}<20 K), massive dust reservoir are still uncertain. In an effort to characterize the very low-metallicity regime, we present new ALMA observations of the dwarf galaxy SBS 0335−052.

1.1 General properties of SBS 0335−052

Among nearby low-metallicity galaxies, the blue compact dwarf SBS 0335−052 at 54 Mpc is one of the best laboratories to study vigorous star formation in quasi-pristine conditions. It is composed of a main body (Fig. 1) that we refer to as SBS 0335−052. Its general properties are listed in Table 1. SBS 0335−052 is well known as one of the lowest metallicity galaxies of the nearby Universe, with $12 + \log(O/H) \sim 7.25$ (Izotov et al. 2009), and exhibits

★ E-mail: dcormier@zah.uni-heidelberg.de

© 2017 The Authors

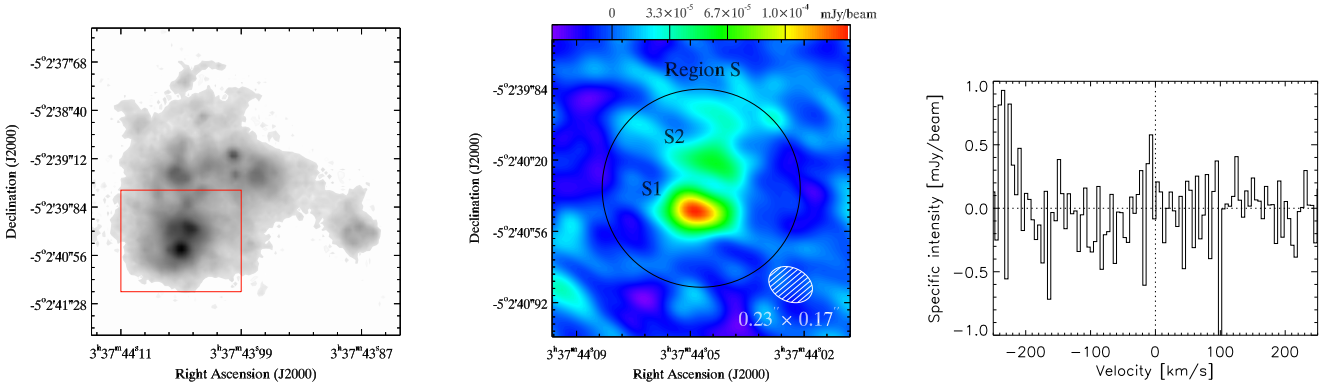

Figure 1. *Left: HST* ACS FR656N map of the main body of SBS 0335−052, downloaded from the Hubble Legacy Archive (http://hla.stsci.edu/), in logarithmic scale. The red box indicates the area shown in the middle panel. *Middle:* ALMA band 6 continuum image in mJy/beam. The beam is shown in white. An aperture of radius 0.5 arcsec encompassing S1 and S2 used for photometry is shown in black (labeled region S, as in Johnson et al. 2009). *Right:* ALMA band 6 CO J=2→1 spectrum averaged within one beam centered at the position of the continuum emission peak (S1). The spectral resolution is 5 km s^{-1}.

exceptionally active star formation, with a total star-formation rate (SFR) of 0.7 $M_\odot$ yr^{-1} (Rémy-Ruyer et al. 2015) and Σ_{SFR} as high as 20 $M_\odot$ yr^{-1} kpc^{-2} (Johnson et al. 2009). Star formation in SBS 0335−052 is located in 6 compact (<60 pc) super star clusters (SSCs; Thuan et al. 1997). The bulk of its stellar population has an age of less than 500 Myr. The two brightest SSCs, located to the south (S1 and S2 on Fig. 1), are the youngest, with ages ≤3 Myr and stellar masses of ∼ 10^6 $M_\odot$ (Reines et al. 2008) each.

ISO and *Spitzer* observations reveal strong mid-IR continuum from warm dust, no polycyclic aromatic hydrocarbons, and hard radiation fields (e.g., Thuan et al. 1999; Wu et al. 2006). While optical studies measure an average visual extinction A_V of ∼0.7 mag (e.g., Izotov et al. 1997; Vanzi et al. 2000; Reines et al. 2008), with values similar in S1 and S2, dust modeling of the unresolved IR emission yields A_V≥10 mag (e.g., Thuan et al. 1999; Hunt et al. 2005). This discrepancy suggests the presence of a separate component with high IR optical depth and probably hidden star formation. Although this galaxy remains undetected in CO (Dale et al. 2001; Hunt et al. 2014), warm molecular gas is present, since near-IR H_2 lines are detected in the southern clusters (e.g., Vanzi et al. 2000).

In this letter, we present new ALMA band 6 observations of SBS 0335−052 at a resolution of 0.2 arcsec (52 pc). Section 2 describes the observations. The molecular gas reservoir and spectral energy distribution are analysed in Sections 3 and 4. We discuss and summarize our results in Sections 5 and 6.

2 DATA

2.1 ALMA band 6 data

Observations of SBS 0335−052 were carried out in 5 blocks between August, 30 2015 and September, 23 2015 as part of the Cycle 2 program 2013.1.00916.S (PI Cormier). We targeted the continuum and ^{12}CO J=2→1 line in band 6 at a spatial resolution of 0.2 arcsec. Observations were made in extended configuration with 35 antennas. The field-of-view is 15 arcsec. One spectral window was centered at a rest frequency of 230.5 GHz with resolution 1.3 km s^{-1} and the 3 other spectral windows were centered at 232.5, 245.5 and 247.5 GHz. Each window has bandwidth of 1.875 GHz. All windows were combined to make the continuum map (total bandwidth of 7.5 GHz centered around 239 GHz).

Table 1. Properties of SBS 0335−052 (E).

General characteristics		
Coordinates (J2000)	03h37m44.0s, -05d02m40s	
Distance	54.1 Mpc	(*)
12 + log(O/H)	7.12-7.32	(1)
$M_{stellar}$	5.6 × 10^6 $M_\odot$	(2)
M_{HI}	4.3 × 10^8 $M_\odot$	(3)
SFR	0.7 $M_\odot$ yr^{-1}	(4)
Σ_{SFR} (region S)	20 $M_\odot$ yr^{-1} kpc^{-2}	(5)
ALMA band 6 observations at 230 GHz		
Continuum (S1)	0.207±0.013 (mJy)	
Continuum (S2)	0.088±0.011 (mJy)	
Continuum (region S)	0.317±0.048 (mJy)	
CO J=2→1	<0.41 (mJy/beam)[a]	

[a] RMS of the spectrum at a spectral resolution of 5 km s^{-1}. (*) Luminosity distance from NED, based on Hα velocity from Moiseev et al. (2010); (1) Izotov et al. (2009); (2) Reines et al. (2008); (3) Ekta et al. (2009); (4) Rémy-Ruyer et al. (2015); (5) Johnson et al. (2009).

We reprocessed and recalibrated the raw data from the archive using the Common Astronomy Software Applications version 4.6.0 (McMullin et al. 2007). Data from each execution block were first processed through a set of standard calibration steps to correct phase and amplitude variations versus time and versus channel and to flux calibrate the data. Data from antennas or channels which have irregular phases or amplitudes are flagged during the calibration. The final images were then created using the CLEAN algorithm with natural weighting. The source was calibrated using quasars where the estimated flux densities have uncertainties of <∼15 per cent. The reconstructed Gaussian beam size in the final images is 0.23 arcsec×0.17 arcsec with a position angle of 65°, which matches the full-width at half maximum of the axes of the beam before deconvolution as well as the axis orientation. The continuum is detected at a signal-to-noise of 10 towards the peak of emission and resolved into two compact knots (S1 and S2, see Fig. 1). We achieve an rms of 0.011 mJy/beam in the continuum. We extract fluxes for the two SSCs by fitting 2D ellipses constrained by the shape of the ALMA beam. We fit each SSC at a time, masking out the other SSC. Emission from S1 is marginally

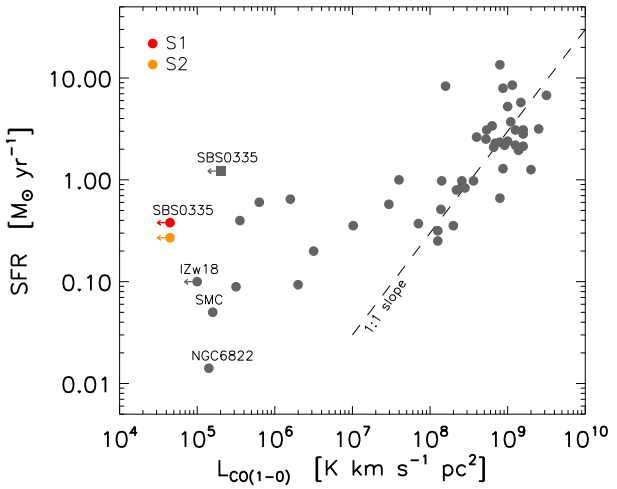

Figure 2. Star-formation rate (SFR) as a function of CO J=1→0 luminosity. Limits are 3-σ. Literature data are in grey, compiled from: Schruba et al. (2012) (circles) and Hunt et al. (2014) (square). To guide the eye, the dashed line indicates a power-law slope of 1. SBS 0335−052 is 10^4 times fainter in CO than a solar-metallicity galaxy exhibiting a similar SFR.

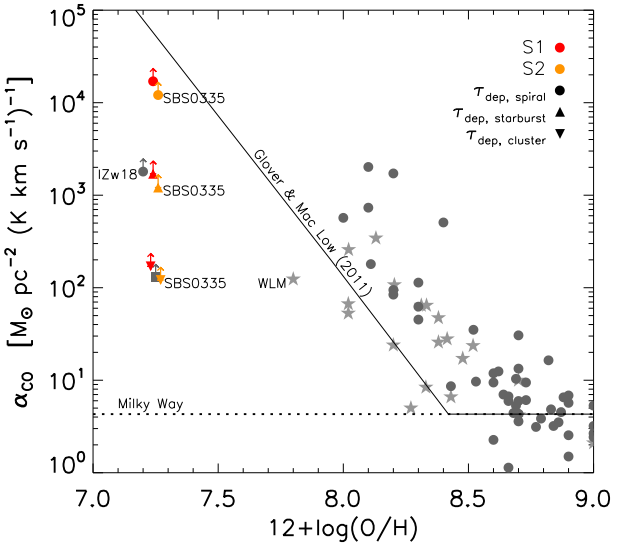

Figure 3. Conversion factor α_{CO} as a function of metallicity. SBS 0335−052: circles, upward triangles, and downward triangles are for τ_{dep} of 2 Gyr, 0.2 Gyr, and 20 Myr respectively. Limits are 3-σ. Literature data points are in grey, compiled from: Schruba et al. (2012) which assumes τ_{dep} of 1.8 Gyr (circles); Hunt et al. (2014) for SBS 0335−052 which assumes a subtended area of 3.5 arcsec^2 and τ_{dep} of ∼7×10^7 yr (square); Israel (1997), Leroy et al. (2011), and Elmegreen et al. (2013) for Local Group dwarf galaxies which use dust continuum emission (stars). We overplot predictions from Glover & Mac Low (2011) where A_V is converted to oxygen abundance assuming a linear scaling (A_V of 3.5 mag corresponds to 12 + log(O/H) = 8.42).

resolved (fitted with an ellipse of size 1.15× the beam). Over the region S, we measure a total flux of 0.32 mJy (Table 1) with a circular aperture of radius 0.5 arcsec covering S1 and S2. The sum of the Gaussians agrees with the total within errors, indicating no significant extended emission. Uncertainties are given as the rms per beam times $\sqrt{N_{\rm beams}}$. The CO J=2→1 line is not detected. We report an rms of 0.41 mJy/beam, for a spectral resolution of 5 km s^{-1}. The maximum recoverable scale of our observations is ∼5 arcsec (∼1.3 kpc), so we are not missing extended emission in our analysis.

2.2 Ancillary data and star-formation rates

We compare our ALMA observations to ISM data of SBS 0335−052 as well as radio data. We use *Herschel* photometry at a resolution >5 arcsec from Rémy-Ruyer et al. (2015). We complement those with ALMA band 7 (346 GHz) data from Hunt et al. (2014) at ∼0.6 arcsec resolution. Additionally, we use radio continuum data from the VLA (1.3 to 6 cm) at ∼0.5 arcsec resolution and SSC-extracted fluxes from Johnson et al. (2009). SBS 0335−052 was observed at 1.5–22 arcsec resolution with the VLA (1.3 to 21 cm) by Hunt et al. (2004). Although SBS 0335−052 is not resolved in the *Herschel* data or in the VLA data from Hunt et al. (2004), there is evidence that S1 and S2 dominate the global emission at other wavelengths. Hence we consider emission from region S as total emission. The total SFR of the galaxy, measured by combining the Hα and total infrared emission, is ∼0.7 M$_\odot$ yr^{-1} (Rémy-Ruyer et al. 2015). From resolved studies, 1.3 cm emission yield SFRs of 0.38 and 0.27 M$_\odot$ yr^{-1} for S1 and S2 (Johnson et al. 2009).

3 STAR FORMATION AND MOLECULAR RESERVOIR

The new ALMA observations put stringent constraints on the amount of CO-emitting molecular gas in SBS 0335−052. Assuming a broad line width of 50 km s^{-1}, as measured from H I (Ekta et al. 2009), we derive a conservative 3-σ $L_{CO(2-1)}$ limit of 3.6 × 10^4 K km s^{-1} pc^2. Our solid angle is 0.044 arcsec^2. Taking a CO(2-1)/CO(1-0) ratio of 0.8 (e.g., Sage et al. 1992), this corresponds to a $L_{CO(1-0)}$ limit of 4.5 × 10^4 K km s^{-1} pc^2. Previous CO J=1→0 and CO J=3→2 measurements by Dale et al. (2001) and Hunt et al. (2014), with solid angles of 23 arcsec^2 and 1 arcsec^2 and a CO(3-2)/CO(1-0) ratio of 0.6, put $L_{CO(1-0)}$ limits of 8.9×10^6 and 1.8×10^5 K km s^{-1} pc^2, respectively. Figure 2 shows the CO J=1→0 luminosity as a function of SFR for SBS 0335−052 and several nearby galaxies which measurements are compiled in Schruba et al. (2012). Our ALMA data provide a new limit on the CO luminosity in SBS 0335−052. SBS 0335−052 clearly stands out in being so CO faint for a star-forming galaxy.

The CO-to-H$_2$ conversion factor (α_{CO}) being unconstrained at low metallicity, we do not convert this luminosity into a limit on the mass of H$_2$. Instead, we hypothesize that star formation proceeds with a given depletion time-scale, τ_{dep}=M(H$_2$)/SFR. We assume three different molecular gas depletion times: 2 Gyr - a common value for normal, disc-type galaxies (e.g., Bigiel et al. 2008); 0.2 Gyr - a common value for starburst galaxies (e.g., Daddi et al. 2010); and 20 Myr - a common value for local molecular clouds (e.g., Lada et al. 2012). Significantly reduced depletion time-scales - similar to starburst values - have been found by Kepley et al. (2016) for another dwarf galaxy, II Zw 40.

From the CO luminosity and SSC-derived SFR values, we can constrain α_{CO}. The α_{CO} limits that we find for S1 and S2 are shown in Figure 3 and are around 10^2 M$_\odot$ pc^{-2} (K km s^{-1})$^{-1}$ for cloud depletion times (20 Myr), and 10^3 − 10^4 M$_\odot$ pc^{-2} (K km s^{-1})$^{-1}$, amongst the highest, for whole-galaxy depletion times (0.2−2 Gyr). The most surprising finding is that, even at our 50 pc resolution, CO is not detected. Glover & Mac Low (2011) analyse variations of the α_{CO} factor as a function of visual extinction in numeri-

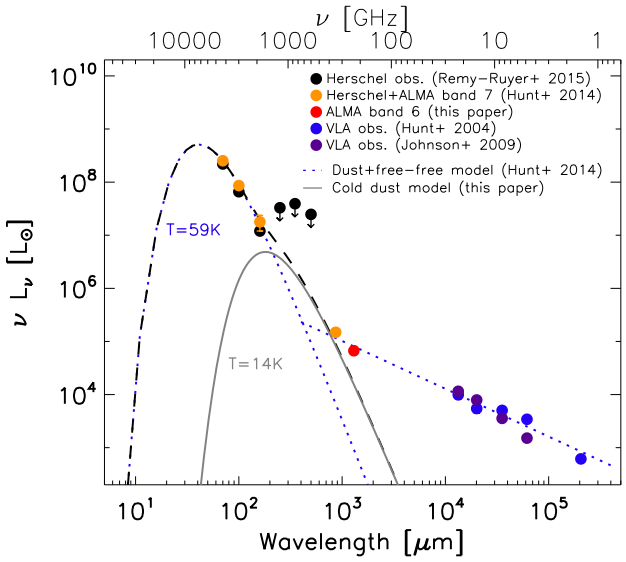

Figure 4. Far-IR-radio Spectral Energy Distribution of SBS 0335−052. The dashed black line shows the total dust model. The individual model components and observations are listed in the legend.

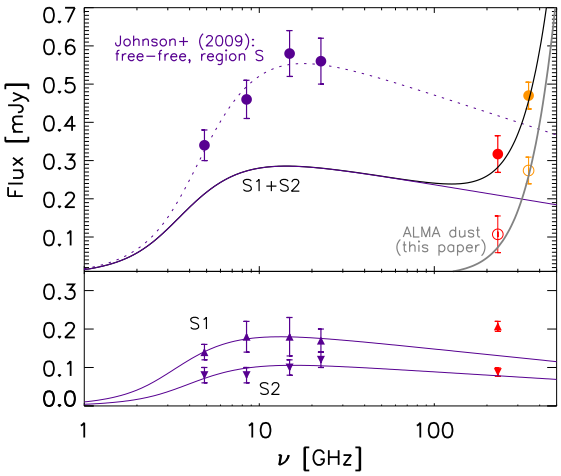

Figure 5. *Top:* Radio SED of SBS 0335−052 for region S with VLA observations from Johnson et al. (2009) in purple, and ALMA data from Hunt et al. (2014) in orange and from this paper in red. The dotted purple line is the free-free model for region S and the plain purple line is the summed free-free models for S1 and S2, from Johnson et al. (2009). The open circles are the ALMA data with free-free emission from S1+S2 subtracted. We model the ALMA data of region S with the free-free models of S1+S2 and a dust component in grey. The full model is shown in black. *Bottom:* SED for the individual clusters S1 and S2 with VLA observations and free-free models from Johnson et al. (2009) in purple and our ALMA data in red.

cal simulations of low-metallicity clouds. Following their study, our results are compatible with mean visual extinctions of 0.1-1 mag. This is within values found from optical data (Izotov et al. 1997; Reines et al. 2008) and much lower than expected from IR data. The filling factor of the shielded and IR-bright component in SBS 0335−052 must be very small. Reines et al. (2008) estimate a clumpy dust covering factor of 60 per cent. With our 1-σ limit of $W_{CO(1-0)} \leq 5\,K\,km\,s^{-1}$ at a resolution of 50 pc, and a typical CO clump brightness of $15\,K\,km\,s^{-1}$ (Glover & Clark 2012), we estimate a beam filling factor for the CO-emitting clumps of less than 33 per cent.

4 SPECTRAL ENERGY DISTRIBUTION

Figure 4 shows the total FIR-radio SED of SBS 0335−052. The photometry consists of *Herschel*, ALMA, and VLA observations. Hunt et al. (2014) model the ALMA 345 GHz and VLA data with free-free emission and the *Herschel* data with warm dust (T_{dust}=59 K). Our ALMA observation (red point) falls slightly below their free-free model. Figure 5 shows a zoom on the radio SED, focusing on the high-resolution data. Johnson et al. (2009) model the emission from S1, S2, and region S with three distinct free-free components. For region S, their model passes in between the ALMA band 6 and band 7 data but disagrees at a >2-σ level from the two observations. Moreover, the ALMA fluxes cannot be reproduced simultaneously with free-free emission only. In particular, the slope between the ALMA bands 7 and 6 is incompatible with gas emission and is rather indicative of thermal dust emission. For S2, the ALMA band 6 data match well the free-free model of Johnson et al. (2009). For S1, our flux at 230 GHz is 1.3 times higher than their model (10-σ significance) and we cannot fit both the VLA and ALMA data within errors with a single free-free model. Therefore in the following we consider an additional dust component that is most visible in S1 and not S2. We investigate the significance of a dust excess by focusing on S1. Fitting the SED of S1 with an additional dust component results in a better χ^2 than without it, and an F-test indicates that the probability of this dust component is high (>98 per cent). This is valid when employing modified black-body spectra as well as more realistic dust optical properties and a distribution of temperatures (Galliano et al. 2011).

To model the dust emission present in the ALMA data of region S, we subtract the free-free emission predicted by the Johnson et al. (2009) models for the clusters S1 and S2. Note that we do not subtract their free-free model for region S (shown for reference in the top panel of Fig. 5) because there are discrepancies in the VLA observations/models of Johnson et al. (2009) and Hunt et al. (2004) for region S and the whole galaxy, respectively, whose origin is not clear to us. Then, we fit a dust component to the ALMA excess of region S (open circles in Fig. 5). We find that the PACS data and ALMA excess cannot be reproduced simultaneously with a single modified black-body (MBB). This remains true even if the PACS data encompass extended emission not belonging to region S. In addition to the MBB fitted to the PACS observations (59 K, $\beta = 2$), we require a second dust component, for which we assume common values of $\kappa_{160} = 1.6\,m^2\,kg^{-1}$ and $\beta = 1.7$ (Galliano et al. 2011). The PACS 160 μm measurement puts an upper limit on the dust temperature of $T_{dust} \leq 14$ K, which gives a mass $M_{dust} \simeq 1.5 \times 10^5\,M_\odot$ (grey lines in Figs. 4 and 5). With a temperature of 10 K, the required mass is $\sim 3 \times 10^5\,M_\odot$. Those dust masses are about 4 times larger than the dust mass of $3.8 \times 10^4\,M_\odot$ found by Hunt et al. (2014) and more than 10 times larger than previous dust estimates based on *Herschel* data only (Rémy-Ruyer et al. 2015). We note that this cold dust mass is an estimate only. In particular, alternative dust properties or mantle coating, resulting in a larger overall emissivity would reduce the mass (e.g., Köhler et al. 2014). It is also possible that the grains could exhibit an intrinsic excess at longer wavelength (e.g., Meny et al. 2007; Coupeaud et al. 2011). Further constraints between 200 μm and 600 μm would be extremely valuable to confirm the cold dust hypothesis.

5 DISCUSSION

SBS 0335−052 is a very intriguing galaxy in the sense that it is actively star-forming, metal-poor, with a large H I reservoir and extremely faint, still undetected CO emission. It potentially harbours a large dust/hidden molecular reservoir. Here we discuss the implications of such massive cold reservoirs on the galaxy properties and theory of star-formation (varying efficiencies, role of H I in metal-poor environments).

Concerning the gas reservoir, with the SFR and τ_{dep} values used in Sect. 3, we find molecular gas masses of 5×10^6–8×10^8 $M_\odot$. This is the mass of gas within S1 and S2 required to explain the current star formation. If the depletion time is long (∼2 Gyr), the inferred molecular mass is larger than the H I mass within region S, estimated to be around $4 \times 10^6 - 10^7$ $M_\odot$ by Ekta et al. (2009) and Hunt et al. (2014), and it is on the order of the total H I mass of 4×10^8 $M_\odot$ (Ekta et al. 2009). If the depletion time is short (∼20 Myr), the inferred molecular mass is of the order of the H I mass in region S and lower than the total H I mass. Recent numerical simulations at low metallicity demonstrate that star formation can happen in a primarily atomic-dominated ISM (Krumholz 2012; Glover & Clark 2016). In the case of very short depletion times, no hidden molecular gas is required in SBS 0335−052 to explain the SFR, while in the case of longer depletion times, a massive amount of hidden molecular gas would be required.

Concerning the dust, the cold material found in Sect. 4 could be responsible for the large extinction ($A_V \simeq 20$ mag) needed in the mid-IR SED modeling. Thuan et al. (1999) estimate the dust surface density to be 1.5 $M_\odot$ pc^{-2}. Since the ALMA emission in S1 is barely resolved, we assume that the cold dust spatial extent corresponds to our beam size. Following the calculations of Thuan et al. (1999) and assuming a uniform dust distribution, the cold dust mass needed to account for the mid-IR extinction is $\sim 5\times10^3$ $M_\odot$, i.e. 30 times lower than our new estimate. This estimate will go up if the dust is distributed in clumps, as suggested by Reines et al. (2008). It is noteworthy that the gas mass that is implied by our new dust estimate, assuming full condensation of the metals into dust, is of the same order of the gas mass estimated assuming τ_{dep} of 2 Gyr. This cold gas mass is a few times larger than the warm H_2 mass of $\sim10^8$ $M_\odot$ (based on modeling of the NIR H_2 lines; Thuan et al. 2005), as found in nearby metal-rich galaxies (e.g., Roussel et al. 2007). Those facts further support our interpretation of an extreme α_{CO} value needed to explain the non-detection of CO emission even with ALMA.

6 CONCLUSION

We present ALMA band 6 (230 GHz) observations in the blue compact dwarf galaxy SBS 0335−052 at an unprecedented resolution of 0.2 arcsec (52 pc). The CO J=2→1 line is not detected. We report a very deep 3-σ $L_{CO(2-1)}$ limit of 3.6×10^4 K km s^{-1} pc^2. This corresponds to a lower limit on the α_{CO} conversion factor of 10^2 $M_\odot$ pc^{-2} (K km s^{-1})$^{-1}$ when assuming cloud depletion times and of $10^3 - 10^4$ $M_\odot$ pc^{-2} (K km s^{-1})$^{-1}$ for whole-galaxy depletion times. The faintness of CO emission implies, for a whole-galaxy star-formation depletion time, a dominant amount of CO-dark gas. The ALMA continuum emission is detected and resolved over the two main SSCs. Re-analysis of the IR-radio SED suggests that the mm-fluxes are not only free-free emission but that there is a cold dust component coincident with the position of S1. Assuming standard dust properties, the dust mass could be as large as 10^5 $M_\odot$. This mass of cold dust corroborates the CO-dark gas interpretation.

ACKNOWLEDGEMENTS

We acknowledge support from the SYMPATICO grant (ANR-11-BS56-0023) of the French Agence Nationale de la Recherche; the DAAD/PROCOPE projects 57210883/35265PE; the DFG for the programmes BI 1546/1-1 and HO 5475/2-1. and for funding in SFB 881 'The Milky Way System' (subprojects B1, B2, and B8) and in SPP 1573 'Physics of the ISM' (grants KL 1358/18.1, KL 1358/19.2); the ERC via the Advanced Grant 'STARLIGHT' (project number 339177). This paper makes use of the following ALMA data: ADS/JAO.ALMA#2013.1.00916.S. ALMA is a partnership of ESO (representing its member states), NSF (USA) and NINS (Japan), together with NRC (Canada), NSC and ASIAA (Taiwan), and KASI (Republic of Korea), in cooperation with the Republic of Chile. The Joint ALMA Observatory is operated by ESO, AUI/NRAO and NAOJ.

References

Bigiel F., Leroy A., Walter F., Brinks E., de Blok W. J. G., Madore B., Thornley M. D., 2008, AJ, 136, 2846
Bolatto A. D., Wolfire M., Leroy A. K., 2013, ARA&A, 51, 207
Cormier D., et al., 2014, A&A, 564, A121
Coupeaud A., et al., 2011, A&A, 535, A124
Daddi E., et al., 2010, ApJ, 714, L118
Dale D. A., Helou G., Neugebauer G., Soifer B. T., Frayer D. T., Condon J. J., 2001, AJ, 122, 1736
Ekta B., Pustilnik S. A., Chengalur J. N., 2009, MNRAS, 397, 963
Elmegreen B. G., Rubio M., Hunter D. A., Verdugo C., Brinks E., Schruba A., 2013, Nature, 495, 487
Galliano F., et al., 2011, A&A, 536, A88
Glover S. C. O., Clark P. C., 2012, MNRAS, 421, 9
Glover S. C. O., Clark P. C., 2016, MNRAS, 456, 3596
Glover S. C. O., Mac Low M.-M., 2011, MNRAS, 412, 337
Hunt L. K., Dyer K. K., Thuan T. X., Ulvestad J. S., 2004, ApJ, 606, 853
Hunt L., Bianchi S., Maiolino R., 2005, A&A, 434, 849
Hunt L. K., et al., 2014, A&A, 561, A49
Hunt L. K., et al., 2015, A&A, 583, A114
Israel F. P., 1997, A&A, 328, 471
Izotov Y. I., Lipovetsky V. A., Chaffee F. H., Foltz C. B., Guseva N. G., Kniazev A. Y., 1997, ApJ, 476, 698
Izotov Y. I., Guseva N. G., Fricke K. J., Papaderos P., 2009, A&A, 503, 61
Johnson K. E., Hunt L. K., Reines A. E., 2009, AJ, 137, 3788
Kepley A. A., Leroy A. K., Johnson K. E., Sandstrom K., Chen C.-H. R., 2016, ApJ, 828, 50
Köhler M., Jones A., Ysard N., 2014, A&A, 565, L9
Krumholz M. R., 2012, ApJ, 759, 9
Lada C. J., Forbrich J., Lombardi M., Alves J. F., 2012, ApJ, 745, 190
Leroy A. K., et al., 2011, ApJ, 737, 12
McMullin J. P., Waters B., Schiebel D., Young W., Golap K., 2007, in Shaw R. A., Hill F., Bell D. J., eds, Astronomical Society of the Pacific Conference Series Vol. 376, Astronomical Data Analysis Software and Systems XVI. p. 127
Meny C., Gromov V., Boudet N., Bernard J.-P., Paradis D., Nayral C., 2007, A&A, 468, 171
Moiseev A. V., Pustilnik S. A., Kniazev A. Y., 2010, MNRAS, 405, 2453
Pilbratt G. L., et al., 2010, A&A, 518, L1+
Reines A. E., Johnson K. E., Hunt L. K., 2008, AJ, 136, 1415
Rémy-Ruyer A., et al., 2015, A&A, 582, A121
Roussel H., et al., 2007, ApJ, 669, 959

Rubio M., Elmegreen B. G., Hunter D. A., Brinks E., Cortes J. R., Cigan P., 2016, preprint, (arXiv:1603.04736)
Sage L. J., Salzer J. J., Loose H.-H., Henkel C., 1992, A&A, 265, 19
Schruba A., et al., 2012, AJ, 143, 138
Thuan T. X., Izotov Y. I., Lipovetsky V. A., 1997, ApJ, 477, 661
Thuan T. X., Lipovetsky V. A., Martin J.-M., Pustilnik S. A., 1999, A&AS, 139, 1
Thuan T. X., Lecavelier des Etangs A., Izotov Y. I., 2005, ApJ, 621, 269
Vanzi L., Hunt L. K., Thuan T. X., Izotov Y. I., 2000, A&A, 363, 493
Wu Y., Charmandaris V., Hao L., Brandl B. R., Bernard-Salas J., Spoon H. W. W., Houck J. R., 2006, ApJ, 639, 157

This paper has been typeset from a TEX/LATEX file prepared by the author.